PROCEEDINGS, 49th Workshop on Geothermal Reservoir Engineering
Stanford University, Stanford, California, February 12-14, 2024
SGP-TR-227

Thermal Hydrological Mechanical Modelling of Anticipated Stimulation in Utah

J Torquil Smith, Eric L Sonnenthal, Nori Nakata

Lawrence Berkeley National Laboratory, Berkeley, California, 94720

jtsmith@lbl.gov

Keywords: enhanced geothermal, stimulation, THM modelling, Utah

ABSTRACT

Additional horizontal wells have been drilled at depth near Milford, Utah. We assume a stimulation plan similar to that used at Blue Mountain, Nevada (Norbeck, Latimer, 2023). We model the stimulation using averaged parameter values from cores from the Utah FORGE site (Ghassemi, Zhou, 2023, McLennan, 2018a). Initial results show extensive fracturing consistent with stimulation results at the nearby Utah FORGE site.

1. INTRODUCTION

A site close to Milford, Utah has been drilled, somewhat deeper than current wells at Utah FORGE, and stimulation is planned to connect parallel horizontal wells with a system of fractures. Here, parameter values obtained from wells at Utah FORGE are used, at a somewhat deeper depth. Following stimulations made at Blue Mountain, Nevada, 12 minutes of injection at 10 bb/min (26.5 kg/s), followed by 155 minutes at 100 bb/min (265 kg/s) spread between six clusters of perforations separated 8.25 m apart (spanning 41.25 m) are simulated. Multiple stages additional of stimulation from similar sets of perforation clusters, offset 49.5 m each, are anticipated, but not modelled here. Thermal and hydrological flow and mechanics including possible simultaneous tensile and Mohr-Coulomb failure are modelled using TReactMech.(Kim et al., 2012, Smith et al., 2015). The code makes a continuum approximation,with failure within an element treated as distributed throughout the element.

2. GRID AND PARAMETER VALUES

The simulation was made on a 96 x 81 x 81 element grid, designed for allowing additional offset stimulations at a later date, covering 1934 m x 625 m x 625 m, with 4.125 m x 5 m x 5m elements in its central zone, expanding roughly geometrically on its edges. The grid is for a zone at depth, entirely in the zone considered roughly granitic (`granitoid') which, at least at the FORGE site, includes some gneiss. The central portion is shown in Figure 1. Initial temperatures and top boundary pressures were values given by Podgorney (2020) centered on the nearby FORGE site, and extrapolated laterally where needed outside the FORGE grid. Initial pressure were assumed hydrostatic relative to the upper domain boundary. An initial 10^6 year flow simulation was made to allow for temperature and pressure stabilization under lateral no flow boundary conditions. Temperatures ranged from 184 to 218 °C at the top and 210 to 250 °C at the bottom. Subsequently, constant pressure, temperature and vertical stress conditions are imposed at the top, constant temperature and pressure and no normal displacement boundary conditions are imposed on the grid sides and front and back, and no vertical displacement, no vertical fluid flow, and constant temperature conditions are imposed at the grid bottom. Injection cells are within the finely gridded portion.

Flow parameter values are given in Table 1. Permeability is an estimate for FORGE well 16(A)(78)-32 (Xing et al., 2021). Porosity is an average of values from FORGE well 58-32 (McLellan, 2018a). Grain density is based on an average well log density of 2686 kg/m^3 in the granitic zone, a porosity of 0.00365 and pore water at 225 °C. Thermal conductivity is from FORGE well 58-32 (Gwynn, et al., 2019). Mechanics parameters are in Table 2. Bulk modulus is an average of values at 26 MPa effective stress (Ghassemi and Zhou, 2022) plus 1 standard deviation. Poisson ratio is an average of values interpolated to 26 MPa effective stress (McLennan, 2018a). Biot coefficient is an average at 26 MPa effective stress (Ghassemi and Zhou, 2022), less 1 standard deviation. Friction angle is a fairly standard value. Mohr-Coulomb dilation angle is a fairly low value for a granitic rock at 26 MPa normal stress (e.g., Kwon, et al., 2019). Sufficient pre-existing (possibly weakly cemented) cracks are assumed so that tensile strength and Mohr-Coulomb cohesion are negligible. The implementation of Mohr-Coulomb failure and tensile failure allows simultaneous failure on multiple fracture planes within an element (Smith et al., 2015). Parameters linking failure porosity and permeability are given in Table 3. Initial permeability is modelled as arising from fractures at the given fracture spacing, with implied aperture derived from a cubic law. For computation of changes in permeability due to further fracturing (failure), failure strain is treated as being on sets of fracture planes and is resolved according to the components of the strain. Changes in fracture porosity due to failure add to the initial fracture aperture, and the resulting permeability is given by the cubic law. The assumed fracture spacing is approximately 4 times the average fracture spacing estimated at FORGE (Finnila et al., 2021) on the assumption that roughly a quarter of fractures contribute to the permeability.

Vertical loading stress at the top of the grid was computed assuming 1978 kg/m^3 density in the upper 359.1 m based on cuttings densities from FORGE well 58-32 between 100 and 300 m depth (Gwynn, et al. 2019), 2443.2 kg/m^3 in the next 1228.3 m, and 2655.6 kg/m^3 below that, to the top of the grid, based on density logs from the site. Within the modelled domain, density was calculated from porosity, grain density and initial fluid density. The ratios of initial stresses were set to 0.657: 0.817: 1 for stress components σ_{xx}:σ_{yy}:σ_{zz} in the minimum and intermediate (horizontal) stress directions and vertical stress. The σ_{xx}: σ_{zz} ratio was based on the average of three stress estimates for FORGE well 58-32 (Xing, et al., 2022), and the σ_{yy}:σ_{zz} ratio was based on an earlier measurement at the FORGE site (McLellan, 2018b). The horizontal minimum stress direction was approximated as east-west (i.e., ±easting direction,

x). Injected water temperature was 4.6 °C, inadvertently below the local mean surface temperature of 10.1 °C, with 12 minutes at 26.5 kg/s, followed by 155 minutes injection at 265 kg/s.

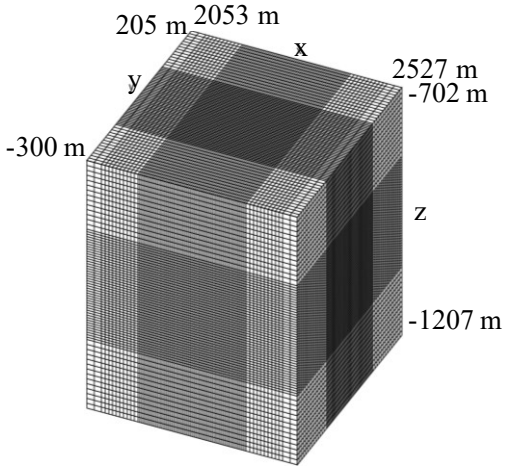

Figure 1: Central 83 x 75 x 75 portion of modelling grid. x=easting, y=northing, z=vertical.

Table 1: Flow parameters.

Grain density	2693 kg/m^3
Initial porosity	0.00543
Initial permeability	2.1 x10^{-17} m^2
Thermal conductivity	2.615 J /°C m
Grain specific heat	1000 J /°C kg

Table 2: Mechanics parameters.

Bulk modulus	26.8 GPa
Poisson ratio	0.2709
(Young's modulus)	36.84 GPa
(Shear modulus)	14.5 GPa
Biot coefficient	0.641
Mohr-Coulomb friction angle	31°
Mohr-Coulomb dilation angle	2°
Lineal thermal expansion coefficient	1.1x10^{-5} /°C

Table 3: Parameters linking failure porosity and permeability

Assumed fracture spacing	4.125 m
Assumed initial fraction of permeability due to fractures	0.999

3. RESULTS

Fluid pressure in six cells adjacent cells in a profile normal to the well, starting at an injection cell, with centers 5 m apart are plotted in Figure 2, for the first 120 minutes of injection. Pressure in the injection cell (solid line) reaches a peak of 84 MPa at 32 s, an increase of 60 MPa over its initial pressure. Pressure in successive adjacent cells increases as fracture reaches them. Some numerical instability is evident in pressures between 12.8 and 19.6 minutes. For comparison, Utah Forge stage 2 stimulation in well 16A(78)-32 showed an

increase of 47 MPa well head pressure after about 2.8 minutes stimulation at 4-10 bb/min, plateauing to about 39 MPa after 110 minutes of injection stepped upwards to 35 bb/min (93 kg/s) (McLennan, 2022). The earlier and higher peak observed is due to simulation fluids being injected directly into elements at depth, which neglects well bore elasticity and compression of well bore fluids. A similar simulation with injection into a well element connected to elements at depth, reduces the initial pressure increase to 48 MPa, and delays it to occur after 6.5 minutes of injection.

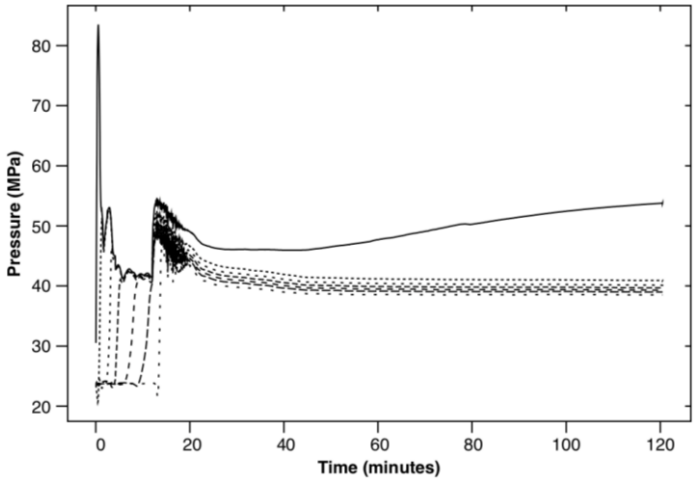

Figure 2. Pressure in six cells adjacent cells, in a profile normal to the well starting at an injection cell, with centers 5 m apart. Solid, injection cell. Dashed, successive cells on 5 m centers, with pressure increasing in one after another in succession.

As an indication of the extent of crack growth, crack volume is plotted as a function of time in Figure 3. Element failure starts on the fourth time step at 5.2 s, but the total crack volume increases fairly slowly until the injection rate is increased by a factor of 10 at 12 minutes.

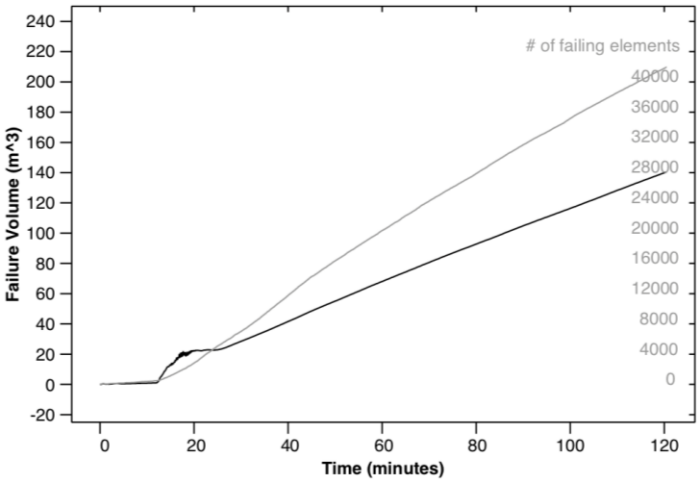

Figure 3. (Black) Failure (crack) volume as a function of time after start of injection. (Grey) number of failing elements,

Crack geometry is somewhat complicated. As expected, the fractured zone runs primarily in the plane normal to the minimum stress direction (x). Isosurfaces of porosity due to failure (induced cracks) after 120 minutes of injection are shown in transparency in Figure 4, looking down, looking west, and looking north. Failure porosity is averaged over grid blocks (e.g. 4.25x5x5 m) so thin cracks appear as low porosity levels. Isosurfaces at 10^{-6} and 10^{-5} levels are almost coincident, so the surface at 10^{-6} is not shown. In transparency, multiple sheets of an isosurface result in a darker color. In particular, the 10^{-5} isosurface shows indentations along the northing axis, as darker zones in the downwards and westward views. Injection points are at the centers of the 10^{-3} level isosurfaces. Departures from east-west symmetry may be due to a combination of differences in grid spacing in the x direction to the two sides of the fractured zone, and due to imprecision in resolution of failure strains. Integrating failure porosity in the minimum stress direction (easting, x) gives an estimate of total crack aperture. This is projected onto a plane in the y and z directions, and its logarithm is plotted at several times in Figure 5. The roughly axially symmetric geometry of the integrated crack aperture roughly resembles some axially symmetric models of hydraulic fracture aperture. The simulation has been run to 50 minutes past the end of injection at 167 minutes, with the fracturing zone extending to 115 x 535 x 375 m, but problems with a simulation restart make results after 120 minutes somewhat speculative and

are not shown. This is greater lateral extent than the approximately 270 m lateral extent seen in micro-earthquakes from Utah FORGE well 16A(78)-32 stimulation 3 (Dyer, et al. 2023), primarily due to the greater volume (12,100 bb) of fluid injected compared to approximately 3,045 bb at FORGE (McLennan, 2022). Element average permeability isosurfaces after 120 minutes of injection are plotted in Figure 6. The 10^{-15} m^2 isosurface strongly resembles to the 10^{-5} porosity isosurface as the permeability change is primarily due to fracturing.

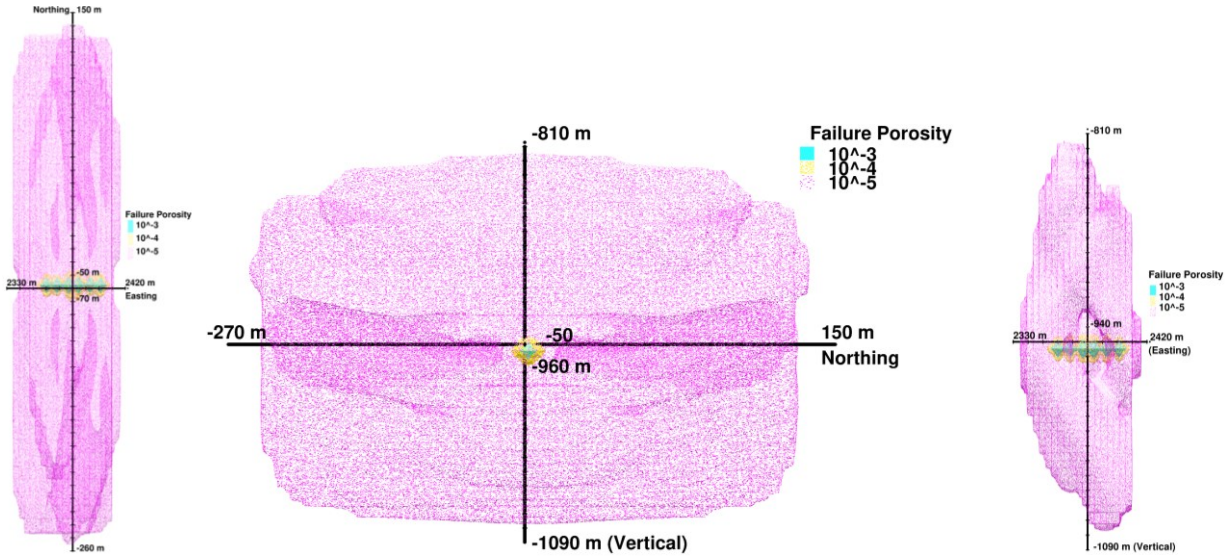

Figure 4. Isosurfaces 10^{-5}, 10^{-4}, and 10^{-3} of failure porosity (induced cracks) after 120 minutes of injection, in transparency; (left) looking down, (middle) looking west, (right) looking north. Injection at 6 centers of 10^{-3} porosity isosurfaces.

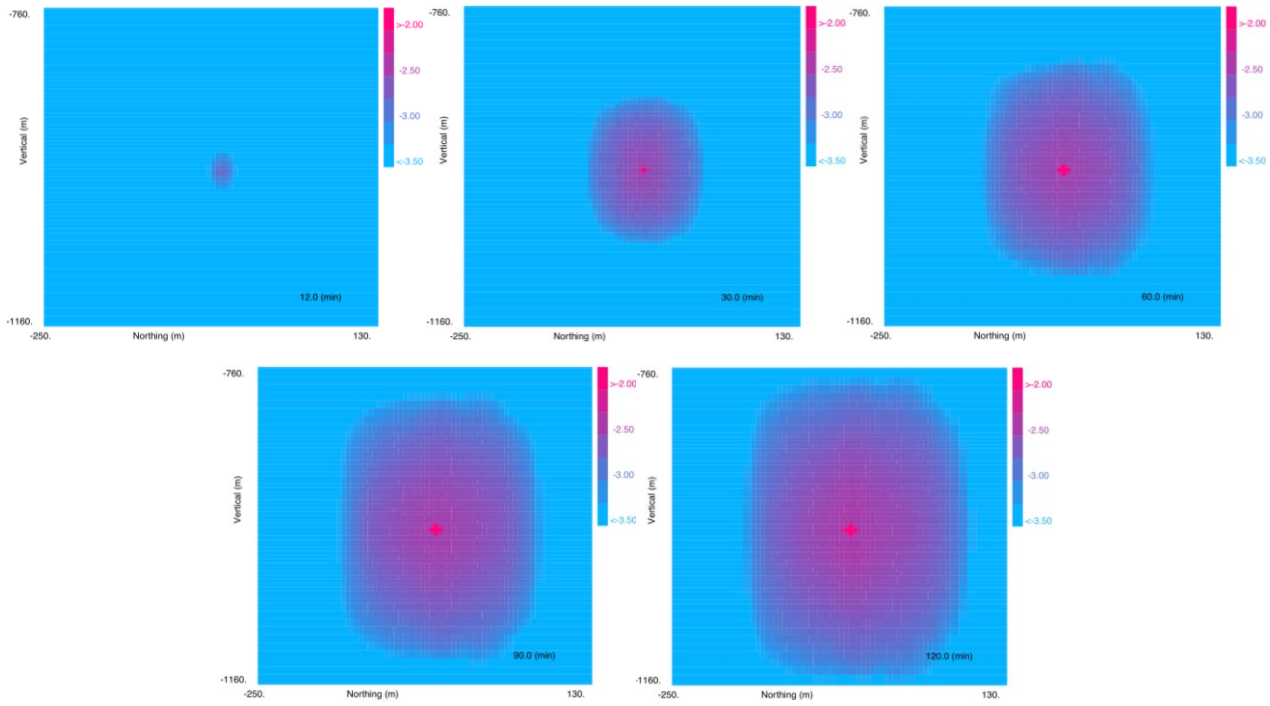

Figure 5. Logarithm$_{10}$ of integrated crack aperture, after 12, 30, 60, 90, and 120 minutes of injection, projected onto y-z plane, from -250 to 130 m easting, and -1160 to -760 m vertical. Line of 6 injection points at cross of high aperture cells.

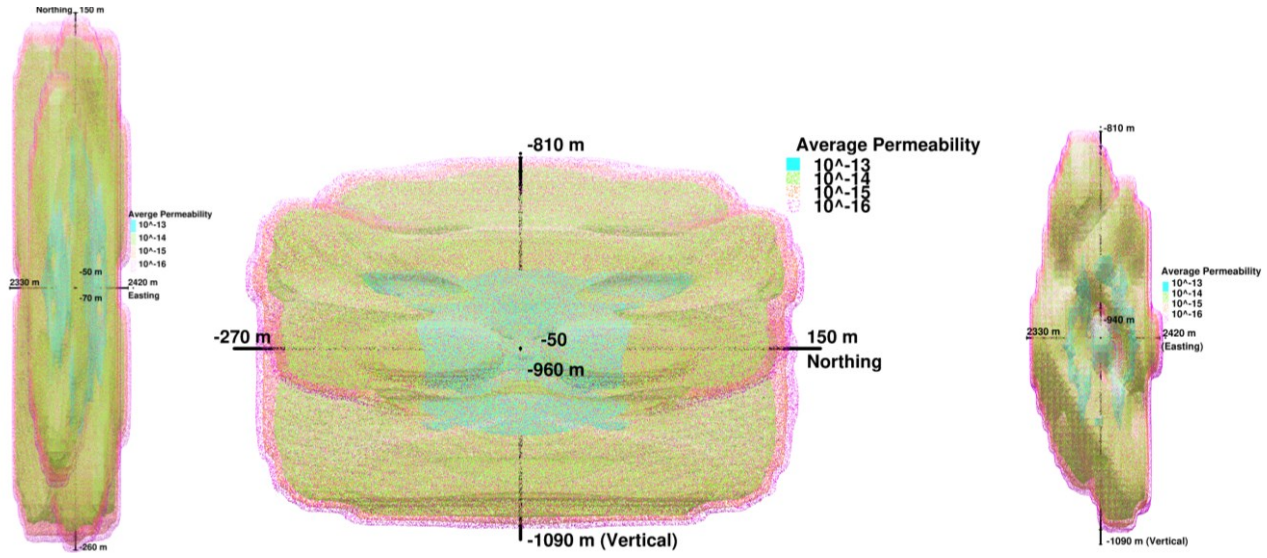

Figure 6. Average permeability (m^2) isosurfaces after 120 minutes of injection, in transparency; (left) looking down, (middle) looking west, (right) looking north.

Shear slip due to failure may be converted directly to seismic moment M (in N-m), via

$$M = A\,\mu\,u \tag{1}$$

where A is area (m^2), μ is shear modulus (Pa), and u is shear displacement (m). In the current case of continuum modelling, shear failure is distributed throughout an element, so for example for xz shear, the net xz failure shear displacement over an element is $\varepsilon_{xy}^{(p)}dz$, where $\varepsilon_{xy}^{(p)}$ is xz failure shear strain and dz is element height, and area $A = dx\,dy$, so $M_{xz} = \varepsilon_{xy}^{(p)}\,dx\,dy\,dz$. This generalizes to all components of failure shear strain, with squared magnitude the sum of the squares of the components. Standard seismic magnitudes are given by $\log_{10}(M)/1.5 - 6.06$. Seismic moment summed over all failing elements is plotted as a function of time in Figure 6 (left). The largest event has magnitude 1, occurring at 12 minutes, at the onset of the higher injection rate. Adding moments cumulatively give the cumulative seismic moment, plotted in Figure 6 (right).

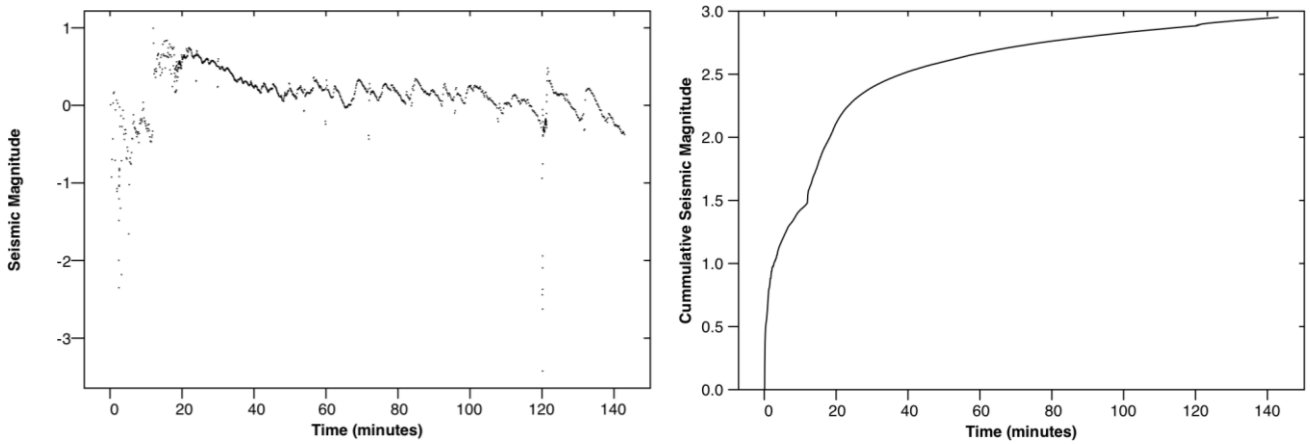

Figure 7. (Left) Seismic moment summed over all failing elements as a function of time, as seismic magnitude. (Right) Cumulative seismic moment, as seismic magnitude.

3. CONCLUSION

Isosurfaces of failure porosity show a somewhat more complex geometry than that of a single opening fracture. Summing crack aperture in the minimum stress direction gives integrated apertures with a roughly axially symmetric profile, reminiscent of axially symmetric models for single hydraulic fracture aperture. During stimulation, isosurfaces of permeability strongly resemble those of fracture porosity since permeability change is primarily due to fracturing. The stimulated zone may exceed 115 x 535 x 375 m, so should produce hydraulic connection to a well 180 m away laterally.

Smith, Sonnenthal and Nakata.

3. ACKNOWLEDGEMENT

This work was supported by the Geothermal Technologies Office of the US. Department of Energy. The authors are grateful to an unspecified company for sharing well bore planning data.

REFERENCES

Dyer, B., Karvounis, D., and Bethmann, F., University of Utah Seismograph Stations. (2022, updated 2023). Utah FORGE Seismic Events Related to the April, 2022 Well 16A(78)-32 Stimulation [data set]. https://gdr.openei.org/files/1429/ Stim_Seis_4_2022.zip

Finnila, A., Doe, T. Podgorney, R., Damjanac, B., Xing, P., Revisions to the discrete fracture network model at Utah FORGE site, GRC Transactions, Vol. 45 (2021).

Ghassemi, A. and Zhou, X., Utah FORGE: Well 58-32 and 78-32 poroelastic properties [data set], University of Oklahoma (2022). https://gdr.openei.org/submissions/1464

Gwynn, M., Allis, R., Hardwick, C. Jones, C., Nielsen, P., and Hurlbut, W. Compilation of rock properties from FORGE well 58-32, Milford, Utah, in Allis, R., and Moore, J.N., editors, Geothermal characteristics of the Roosevelt Hot Springs system and adjacent FORGE EGS site, Milford, Utah: Utah Geological Survey Miscellaneous Publication (2019). 169-L, 36 p., https://doi.org/10.34191/MP-169-L

Kim, J., Sonnenthal, E.L., and Rutqvist, J., 2012, "Formulation and sequential numerical algorithms of coupled fluid/heat flow and geomechanics for multiple porosity materials", Int. J. Numer. Meth. Engng., 92, pp 425-456.

Kwon, S., Xie, L., Park, S., Kwang-Il, K., Ki-Bok, M., et al., Characterization of 4.2-km-deep fractured granodiorite cores from Pohang geothermal reservoir, Korea. Rock Mechanical and Rock Engineering, (2019), vol. 52 (1), 771-782.

McLennan, J., Utah FORGE: Well 58-32 Core Analyses, Energy and Geoscience Institute at the University of Utah (2018a, updated 2020). https://gdr.openei.org/submissions/1162.

McLennan, J., Stress measurements MU-ESW1 (performed Sept 22-23, 2017), in Utah FORGE: Well 58-32 Core Analyses, Energy and Geoscience Institute at the University of Utah (2018b, updated 2020). https://gdr.openei.org/submissions/1162.

McLennan, J., Utah FORGE Well 16A(78)-32 stimulation data (April, 2022), Energy and Geoscience Institute at the University of Utah. (2022). Utah FORGE Well 16A(78)-32 Stimulation Data (April, 2022) [data set]. Retrieved from https://dx.doi.org/10.15121/1871203. https://gdr.openei.org/files/1379/16A78-32_Stimulation_Stage%202.zip.

Podgorney, R.: Utah FORGE: Data for 3-D Model Development - Lithology, Temperature, Pressure, and Stress [data set]. Idaho National Laboratory (2020). https://gdr.openei.org/submissions/1205

Smith, J.T., Sonnenthal, E.L., and Cladouhos, T.: Thermal-Hydrological-Mechanical Modelling of Shear Stimulation at Newberry Volcano, Oregon. *Proceedings of 49th US Rock Mechanics/Geomechanics Symposium*, American Rock Mechanics Association, ARMA 15-0680, (2015).

Xing, P., McLennan, J., and Moor, J., In-situ stress measurements at the Utah frontier observatory for research in geothermal energy (FORGE) site, Energies (2020), vol 13, no. 21, 5842. https://doi.org/10.3390/en13215842.

Xing, P. Winkler, D., Swearingen, L., Moore, J., McLennan, J. In-situ stresses and permeability measurements from testings in injection well 16A(78)-32 at Utah FORGE site, GRC Transactions (2021), vol. 45, pp871-884.